Physicochemical Properties of (R)- vs (S)-Methylphosphonate Substitution on Antisense DNA Hybridization Determined by Free Energy Perturbation and Molecular Dynamics

F. H. Hausheer,*,† B. G. Rao,‡ J. D. Saxe,§ and U. C. Singh⊥

Contribution from The Molecular Design Laboratory, The Cancer Therapy and Research Center, San Antonio, Texas 78229, Medical Oncology Division, University of Texas Health Sciences Center, San Antonio, Texas 78229, Vertex Pharmaceuticals, Inc., Cambridge, Massachusetts 02139-4211, Sterling Research Group, Malvern, Pennsylvania 19355, and Scripps Clinic and Research Foundation, La Jolla, California 92037. *Received August 19, 1991*

Abstract: Methylphosphonate (MP)-substituted antisense DNA oligomers have significant potential for genome targeted therapy. The physicochemical basis of the difference in *R*- versus *S*-MP diastereomers incorporated into DNA oligomers with regard to complementary DNA target hybridization has been poorly understood. State of the art advanced molecular computational methods and supercomputer technology were applied to identify key physicochemical determinants involved in stabilizing and destabilizing target hybridization. MP-oligomer:DNA target hybridization is more stable with *R*-MP substitution and is due to favorable hydrophobic interactions between the equatorial projecting methyl group and water molecules. *S*-MP destabilizes the double strand helix formation by less favorable local hydrophobic interactions with waters, which result in DNA helix unwinding, and by promoting local changes from C2′ endo to C3′ endo in the 5′ furanose ring. In the oligomer studied, R-MP thymine is more stable than R-MP uracil, resulting from hydrophobic interaction to locally stabilize the helix due to the presence of the pyrimidine C5 methyl group. The presence of the C5 methyl group in thymine also appears to influence helical winding and the local conformation of the furanose ring. These numerical simulations are supported by experimental data, enabling us to propose several mechanisms which underlie some of the experimental observations. These results support further development of diastereomerically pure MP analogues as diagnostic/therapeutic agents involving sequence-specific DNA interactions.

Introduction

Nuclease-resistant nonionic oligodeoxynucleotides consisting of a methylphosphonate (MP) backbone have been tested in vitro and in vivo as potential anticancer, antiviral, and antibacterial agents.[1-5] The 5′-3′ linked internucleotide bonds of these analogues closely approximate the conformation of nucleic acid phosphodiester bonds. The phosphate backbone is rendered neutral by methyl substitution of one anionic phosphoryl oxygen. MP-substituted oligomers can penetrate living cells and have been shown to inhibit mRNA translation in globin synthesis and vesicular stomatitis viral protein synthesis and inhibit splicing of pre-mRNA in inhibition of HSV replication.[1-5]

It has been known for nearly a decade that *R*-MP substitutions in DNA oligomers result in more stable complementary binding, as evidenced by an increase in Tm, than *S*-MP diastereomer substitutions.[1] However, fundamental physicochemical mechanisms explaining the greater stability of *R*-MP have not been characterized. Bower et al.[6] suggested that the stability of the MP-substituted DNA is affected by the following three factors: (1) elimination of the phosphate negative charge, (2) electronic and substituent effects, and (3) the steric effect of the MP-methyl group. These investigators proposed that the greater stability of the *R*-MP in comparison to the *S*-MP substitution is due to unfavorable steric interactions of the methyl group in the latter. Lesnikowski et al.[7] synthesized two thymidine methylphosphonates, each composed of *R*-MP and *S*-MP diastereomers of known absolute configuration, and characterized the binding properties. Their results validated the previous observations of other investigators with regard to the modulation of the binding properties of the methylphosphonate-substituted oligomer. There has not been experimental characterization of the structural nature of this interaction which would lead to an explanation of the difference in the binding properties of methylphosphonate diastereomer substitutions.

We have performed large-scale numerical simulations which require Cray supercomputer class hardware to study the physicochemical properties of MP-substituted DNA in triple helices and neutral double strand DNA heteropolymers.[8-10] We have observed that the MP substituent alters the behavior of DNA oligomers in water, and from this work we described the underlying electrostatic, solvation, and conformational properties of the MP substitution in DNA oligomers bound within double strand and triple strand helical complexes. Specifically, it has been observed that the charge neutralization and increase in the hydrophobic character of the phosphate backbone significantly reduces the hydration of the phosphate group in MP-substituted DNA. Therefore, it is possible that the hydration of the phosphate backbone may be different between *R*-MP- and *S*-MP-substituted DNA, and it may contribute to the difference in their hybridization stability. In the present study, we are interested in investigating the nature of different physicochemical interactions affecting the stabilities of MP-substituted DNA oligomers. The experimental quantity used most often to compare the stability of different DNA molecules is the melting temperature which provides limited information, especially with regard to structural transitions that may occur during hybridization and melting.

We were interested in extending our work to develop accurate, numerical models capable of studying the effect of *R*- versus *S*-MP substitution in a more quantitative and chemically useful manner

* The Cancer Therapy and Research Center.
† University of Texas Health Sciences Center.
‡ Vertex Pharmaceuticals, Inc.
⊥ Scripps Clinic and Research Foundation.

(1) Miller, P. S.; Dreon, N.; Pulford, S. M.; McParland, K. B. *J. Biol. Chem.* **1980**, *255*, 9659-9665.
(2) Durand, M.; Maurizot, J. C.; Asseline, U.; Barbier, C.; Thuong, N. T.; Helene, C. *Nucl. Acids Res.* **1989**, *17*, 1823-1837.
(3) Miller, P. S.; Ts'o, P. O. P. *Anti-Cancer Drug Des.* **1987**, *2*, 117-128.
(4) Murakami, A.; Blake, K. R.; Miller, P. S. *Biochemistry* **1985**, *24*, 4041-4046.
(5) Smith, C. C.; Aurelian, L.; Reddy, M. P.; Miller, P. S.; Ts'o, P. O. P. *Proc. Natl. Acad. Sci. U.S.A.* **1986**, *23*, 2787-2791.
(6) Bower, M.; Summers, M. F.; Powell, C.; Shinozuka, K.; Regan, J. B.; Zon, G.; Wilson, W. D. *Nucl. Acids Res.* **1987**, *1*, 4915-4930.
(7) Lesnikowski, Z. J.; Jaworska, M.; Stec, W. J. *Nucl. Acids Res.* **1990**, *18*, 2109-2115.
(8) Hausheer, F. H.; Singh, U. C.; Saxe, J. D.; Colvin, O. M.; Ts'o, P. O. P. *Anti-Cancer Drug Des.* **1990**, *5*, 159-167.
(9) Hausheer, F. H.; Singh, U. C.; Saxe, J. D.; Colvin, O. M.; Ts'o, P. O. P. *Am. Assoc. Cancer Res.* **1989**, *30*, 629.
(10) Hausheer, F. H.; Singh, U. C.; Palmer, T. C.; Saxe, J. D. *J. Am. Chem. Soc.* **1990**, *112*, 9468-9474.

0002-7863/92/1514-3201$03.00/0 © 1992 American Chemical Society

in DNA oligomers by the use of advanced molecular computational methods. Specifically, we were interested in developing numerical models capable of calculating the difference in the Gibbs free energy of hybridization of *R*- versus *S*-MP-substituted oligomers binding to a complementary single strand DNA target. Free energy perturbation calculations have been applied successfully to study a variety of problems. The direct calculation of the relative change in free energy of hybridization as a function of *R*-MP versus *S*-MP substitution could provide a detailed understanding of the physicochemical determinants of MP-diastereomer substitution with regard to hybridization stability. Careful development of reliable numerical simulation methods and molecular models would enable the direct calculation of the Gibbs free energy of oligomer hybridization. The direct calculation of the relative difference in free energy of hybridization comparing two different chemical species would provide a detailed understanding of the physicochemical determinants of MP-diastereomer substitution with regard to hybridization stability, and this information could be used to design oligomers that have superior target hybridization.

In the present study, the antisense oligomer d-[TpTrCrGrTr*CrCrTrC] and the complementary DNA target d[GAGGACGAA] sequence were used for studying two mutations. In the first simulation *R*-MP is mutated to *S*-MP at the site marked by the asterisk in the antisense oligomer. In the second simulation, thymines at two sites (T) are mutated into uracil. The primary purpose of performing these supercomputer simulations is as follows: (1) to determine if large-scale free energy perturbation simulations of antisense DNA hybridization affinities are capable of yielding qualitatively useful information, (2) to understand the molecular mechanism(s) underlying stabilization and destabilization of the oligomer to the target as a function of *R*-MP versus *S*-MP-diastereomer substitution, and (3) to determine if there are local interactions between thymine methyl groups and *R*-MP versus *S*-MP substitutions that could further influence the stability of oligomer hybridization to the target. If successful, this information would be useful in guiding future experimental approaches in designing antisense oligomers possessing more favorable target binding properties.

Methods

Ab Initio Quantum Mechanical Calculations. Geometry optimization and partial atomic charges fitted to the molecular electrostatic potential for the methylphosphonate dimethyl ester fragment were calculated by ab initio quantum mechanical methods with QUEST, version 1.1,[11] using RHF 3-21G* and 6-31G* basis sets,[12] respectively. The latter basis set was used to maintain uniform electrostatic charge assignments with those previously calculated for nucleic acids[10] in the AMBER database. The final monopole atomic charge assignments for the MP fragments were made to obtain a neutral net charge for each base, furanose, and MP diester molecular subunits in the DNA oligomer using published data for the *R*- and *S*-MP substitution. The geometries, ESP charges, and parameters for the MP molecular fragments used in these simulations were taken from previously published data.[8,10]

Molecular Mechanics, Dynamics, and Free Energy Simulations. The molecular mechanics, molecular dynamics, and free energy calculations were carried out using AMBER, version 3.3.[13] The free energy differences were calculated by the free energy perturbation method.[14-16] Determination of binding free energy differences, in general, requires two sets of calculations to complete the thermodynamic cycle given below.

Starting geometries for the DNA duplexes were generated from B-DNA X-ray structures.[17] Two DNA helical complexes were constructed for free energy simulations: (1) calculation of the free energy difference between a single *R*-MP to *S*-MP perturbation (at the position denoted by the asterisk in the oligomer) and (2) the free energy difference between thymine and uracil (two T nucleotides) in an *R*-MP-substituted oligomer.

The negative charge of the native phosphodiester backbone was rendered neutral by placement of positively charged monovalent counterions within 4 Å of the phosphorus atoms bisecting the anionic phosphate oxygens; counterions were not placed in a coordination geometry on the MP-substituted phosphorus atom. The DNA and counterions were surrounded by a 10-Å shell of TIP3P water molecules[18] within a sphere of water 59 Å in diameter (average total volume of each system was 96 966.8 Å^3). The average total number of atoms in each system was 8144. Initially, the DNA and counterion atoms were fully constrained while the surrounding water molecules were energy minimized using a 10.0-A nonbonded cutoff for 2500 cycles. The DNA, counterions, and water were subsequently energy minimized without geometric constraints for an additional 1500 iterations, followed by 220 cycles of minimization with SHAKE[19] bond constraints activated to acclimate the ensemble for molecular dynamics. Molecular dynamics equilibration of each system using SHAKE bond constraints to enable a larger time step of 0.002 ps at constant temperature and pressure (300 K and 1 bar) was carried out within a 10-ps trajectory in each of the molecular ensembles. During molecular dynamics and free energy simulations waters displaced beyond the peripheral boundary (radius = 29.5 Å) of the water sphere were restored to the peripheral boundary position by a half-harmonic force constant of 1.5 kcal/mol. Free energy perturbation simulations were carried out using the window method. Five hundred steps of equilibration (0.002-ps timestep) and 500 steps of data collection (0.002-ps timestep) were performed at each window for 101 windows (total trajectory is 202 ps in each direction of the chemical perturbation). There were no artifacts due to inaccuracies in numerical integration, and the equilibration of the systems at each incremental perturbation of the systems remained within acceptable limits (root-mean-square fluctuations of temperature less than 6 K and less than 1% of the total potential energy of each system). The calculations were made with a fully vectorized version of AMBER, using an all-atom force field. All calculations were performed on CRAY X-MP/24 and CRAY X-MP 1-16/SE supercomputers.

Free Energy Perturbation Method. In the free energy perturbation method, two chemical states (A and B) of a system are represented by the Hamiltonians H_A and H_B, respectively. The transition from one chemical state to another is smoothly carried out by a single coupling parameter, λ, in the following manner:

$$H_\lambda = \lambda H_A + (1 - \lambda)H_B \quad 0 < \lambda < 1$$

This method enables chemical perturbation from state A to state B in a smooth manner by changing the value of λ to produce many partitions of equilibration, followed by statistical sampling during molecular dynamics. The Gibbs free energy change at each step is computed as

$$\Delta G\lambda = -1/\beta \ln \langle \exp(-\beta H_\lambda) \rangle_0$$

where $\beta = 1/RT$. The average of $\exp(-\beta H\lambda)$ is computed over the unperturbed ensemble of the system after equilibration during molecular dynamics. If the perturbation from $\lambda = 1$ to 0 is carried out over N steps, then the total free energy change is given by the following sum of the incremental change in the Gibbs free energy difference of the system (represented by $\Delta G\lambda i$):

$$\Delta G = \sum_{\lambda=1}^{N} \Delta G\lambda i$$

For computing differences in free energies of hybridization, $\Delta\Delta G_{hybrid}$, between the two strands of the DNA with one strand (S_{oligo} and R_{oligo}) undergoing *R*-MP to *S*-MP perturbation hybridized to a target DNA strand (T_{DNA}), the following thermodynamic cycle is employed:

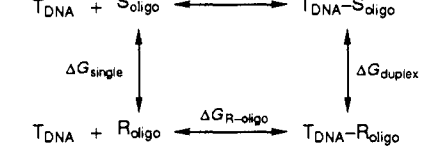

$\Delta\Delta G_{hybrid} = \Delta G_{R\text{-}oligo} - \Delta G_{S\text{-}oligo} = \Delta G_{duplex} - \Delta G_{single}$, where $\Delta G_{R\text{-}oligo}$ and

(11) Singh, U. C.; Kollman, P. A. *J. Comp. Chem.* **1984**, *2*, 129–145.
(12) (a) 3-21G basis set: Binkley, J. S.; Pople, J. A.; Hehre, W. J. *J. Am. Chem. Soc.* **1980**, *102*, 939. (b) 6-31G* basis set: Hariharan, P. C.; Pople, J. A. *Theor. Chim. Acta* **1973**, *28*, 213.
(13) Singh, U. C.; Weiner, P. K.; Seibel, G.; Kollman, P. A. AMBER version 3.3, 1989.
(14) Zwanzig, R. W. *J. Chem. Phys.* **1954**, *22*, 1420–1426.
(15) Singh, U. C.; Brown, F. K.; Bash, P. A.; Kollman, P. A. *J. Am. Chem. Soc.* **1987**, *109*, 1607–1614.
(16) Rao, G.; Singh, U. C. *J. Am. Chem. Soc.* **1989**, *111*, 3125–3133.
(17) Arnott, S.; Hukins, D. W. L. *Biochem. Biophys. Res. Commun.* **1972**, *47*, 1504–1510.
(18) Jorgensen, W. L.; Chandrasekkar, J.; Madura, J. D. *J. Chem. Phys.* **1983**, *79*, 926–935.
(19) Van Gunstersen, W. F.; Berendsen, H. J. C. *Mol. Phys.* **1977**, *34*, 1311–1327.

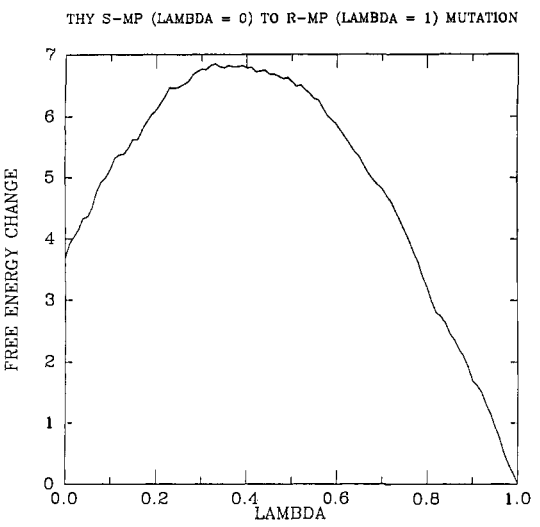

Figure 1. Free energy perturbation profile of *S*-MP to *R*-MP at 300 K in water over a 200-ps molecular dynamics trajectory.

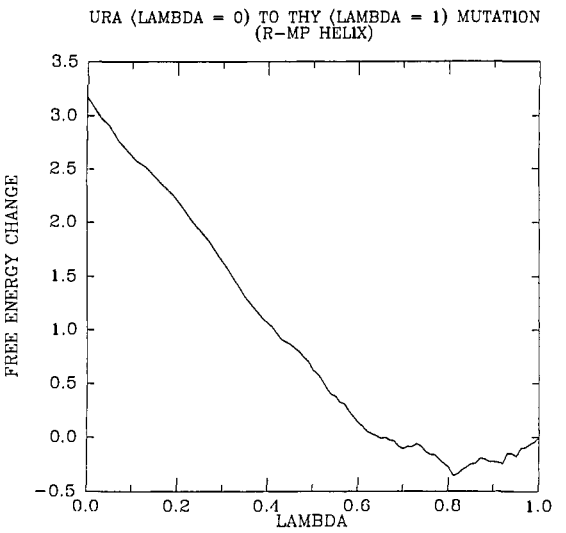

Figure 2. Free energy perturbation profile of thymine to uracil at 300 K in water over a 200-ps molecular dynamics trajectory.

Table I. Hybridization Free Energies ($\Delta\Delta G_{hybrid}$, kcal) of Methylphosphonate-Substituted Oligomers [3′-CrTrCrCr*TrGrCrTpT-5′] Binding to a Complementary DNA Target [5′-GpApGpGpApCpGpApA-3] in Water at 300 K from 200-ps Molecular Dynamics Trajectories

oligomer perturbation	thymine *R*-MP → *S*-MP	*R*-MP thymine → uracil
$\Delta\Delta G_{forward}$	3.7	1.5
$\Delta\Delta G_{reverse}$	−3.5	−1.5
$\Delta\Delta G_{mean}$	3.6	1.5
hysteresis	0.1	<0.1

$\Delta G_{S\text{-}oligo}$ are the (experimental) free energy changes for the hybridization of the strands S_{oligo} and R_{oligo} with the target strand T_{DNA}, respectively, and ΔG_{single} and ΔG_{duplex} are the calculated free energy changes for the mutation of the strand S_{oligo} and R_{oligo} as a monomer in solution and as a double stranded DNA with the target strand T_{DNA} in solution, respectively.

The solvation free energy difference, ΔG_{sol}, of the *R*-MP to *S*-MP perturbation within the free single strand DNA oligomer is expected to be close to zero. Therefore, the value of ΔG_{duplex} will be nearly the same as that calculated by $\Delta\Delta G_{hybrid}$. It is also important to note the difficulty inherent to simulating single strand DNA because of the great flexibility of such molecules. Hence, we have not performed the direct calculation of ΔG_{sol} of this mutation. For the case of the thymine-to-uracil mutation, the same basic approximation is made, although it is not entirely complete in the thermodynamic construct (e.g., treating ΔG_{sol} as zero). At this juncture, it is important to note that the experimental data used for comparison with the calculated values for these mutations are measured Tm values. In this instance a single set of calculations for ΔG_{duplex} for extrapolation to $\Delta\Delta G_{hybrid}$ for each mutation in the double stranded DNA complex in solution was appropriate for studying these problems.

Results

The calculated Gibbs free energy change for hybridization, $\Delta\Delta G_{hybrid}$, of a single *R*-MP ($\lambda = 1.0$) to *S*-MP ($\lambda = 0.0$) perturbation in the antisense oligomer is 3.6 kcal/mol (Figure 1 and Table I). Note in Figure 1 that the free energy profile has a steep positive curve as the single mutation proceeds from *R*-MP to *S*-MP. At $\lambda = 0.5$ the free energy curve decreases in value until $\lambda = 0.0$. The pattern of this free energy profile is due to the stereochemical nature of the perturbation and the physicochemical transitions that occur over the perturbation trajectory. At $\lambda = 0.5$ the antisense oligomer consists of a 50:50 hybrid of a *R*-MP and *S*-MP point perturbation within the oligomer and is equivalent to having two methyl groups symmetrically positioned and superimposed over the two sp^2-hybridized oxygens bonded to the phosphorus atom. The presence of two methyl groups on the phosphorus atom profoundly decreases the availability of sp^2-hybridized phosphoryl oxygens for solvation and hydrogen bonding to surrounding waters and significantly reduces the hydration of the single anionic phosphoryl oxygen of the MP phosphate group from two waters to none. As the perturbation of λ approaches 0.0 (*S*-MP), the availability of the oppositely positioned anionic phosphoryl oxygen increases and concurrently reverses the extreme hydrophobic effect observed at $\lambda = 0.5$ as evidenced by the negative slope of the change in the free energy of the system.

Table II. Average Helical Repeat Angles (in deg) of Oligomers:DNA Hybrids as a Function of *R*-MP versus *S*-MP Substitution in d[TpTrCrGrTr*CrCrTrC] during 200-ps Molecular Dynamics Trajectories in Water at 300 K

base pair	*R*-MP	base pair	*S*-MP
A4–T35	34.8	A4–T35	25.2
G6–C33	28.0	G6–C33	29.4
G8–C31	36.1	G8–C31	22.4
A10–T29*	43.2	A10–T29*	25.7
C12–G27	35.2	C12–G27	32.5
G14–C25	25.7	G14–C25	21.5
A16–T23	42.7	A16–T23	35.5
average =	35.1		27.4
no. of base pairs/turn =	10.2		13.1

The Gibbs free energy profile calculating the value of $\Delta\Delta G_{hybrid}$ for thymine ($\lambda = 1.0$) to uracil ($\lambda = 0.0$) perturbation within an *R*-MP-substituted antisense oligomer hybridized to the complementary DNA target sequence is shown in Figure 2. The net Gibbs free energy change is consistent with an increase in dsDNA helix stabilization by 1.5 kcal/mol accompanying thymine substitution within the antisense oligomer (Table I). Note that as the C5 pyrimidine methyl group is perturbed to hydrogen ($\lambda = 0.5$) the incremental free energy change of $\Delta\Delta G_{hybrid}$ increases steeply in the positive direction. This result suggests that a key function of the C5 methyl group in thymine is to stabilize hybridization of the *R*-MP-substituted oligomer to the complementary single strand DNA target, which is likely predominantly due to hydrophobic driving forces between the surrounding waters and the methyl group. This free energy profile is typical for chemical perturbations involving hydrophobic substituents in water.[15,16]

Analysis of the time averaged DNA coordinates, using the data from 200 images of the coordinate systems obtained at 1-ps intervals, was carried out to study the DNA helical twist conformations as a function of *R*-MP → *S*-MP and for thymine → uracil perturbations, which are given in Tables II and III, respectively. It is important to note that because these are non-identical perturbations of the chemical state, the systems cannot be directly compared because they are identical only when $\lambda = 1.0$ and cease to be identical as the system is perturbed into a different chemical state. These data are useful for identifying conformational transitions as a function of λ, and as such are helpful in char-

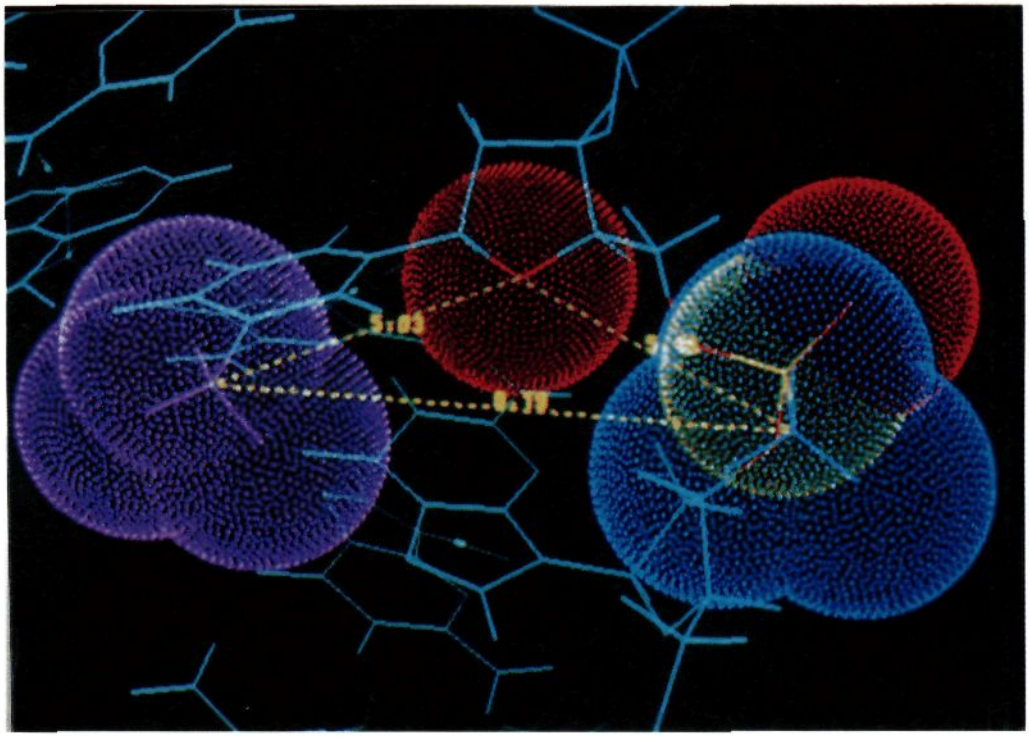

Figure 3. Conformation of the time-averaged geometry of the *S*-MP group attached to the furanose and thymine. The time-averaged conformation from the dynamics trajectory of the *S*-MP group in the DNA oligomer illustrates the close proximity of the methyl group of thymine and the MP moiety. The van der Waals surface of the methyl group of the MP moiety (blue) is anterior to the phosphorus atom (yellow) and the O1′ oxygen atom and phosphoryl oxygen (both shown in red). The close proximity of the methyl groups located on the major groove side of the DNA relative to the O1′ atom is illustrated.

Table III. Average Helical Repeat Angles (in deg) of Oligomers:DNA Hybrids as a Function of Thymine versus Uracil Substitution in d[TpTrCrGrTr*CrCrTrC] during 200-ps Molecular Dynamics Trajectories in Water at 300 K[a]

base pair	thymine	base pair	uracil
A4–T35*	28.9	A4–U35*	37.6
G6–C33	49.2	G6–C33	30.7
G8–C31	17.5	G8–C31	23.5
A10–T29*	22.2	A10–U29*	29.8
C12–G27	64.8	C12–G27	41.0
G14–C25	19.9	C14–C25	20.0
A16–T23	37.5	A16–T23	41.0
average =	34.2		31.9
no. of base pairs/turn =	10.5		11.2

[a] Perturbed bases are underlined.

acterizing the key transitions of the system as a function of the chemical state. The DNA helical complex unwinds in the *S*-MP perturbation, and to a lesser extent in the case of the uracil-substituted helix, as evidenced by the increase in the number of base pairs per 360° rotation of the helix. The *R*-MP substitution allows the hybridized methylphosphonate-substituted oligomer conformation to match that of the complementary DNA oligomer, resulting in minimal distortion of the DNA helical complex relative to that of native B-DNA (~10.0 base pairs per 360° rotation). The single *S*-MP substitution unwinds the DNA oligomer by an average of −7.7°, which represents an increase in 2.9 base pairs per helical turn relative to the *R*-MP substitution. DNA helix unwinding is also observed in the case of the uracil-substituted oligomer, albeit to a lesser degree (average decrease in the helical repeat angle is −2.3°).

Analysis of the time averaged furanose conformations for the corresponding perturbed systems are shown in Tables IV and V. As the perturbation proceeds from *R*-MP to *S*-MP two sugars in the *S*-MP oligomer adopt a C3′ endo conformation. The C3′ endo furanose conformation is consistent with that of A-DNA. As thymine is perturbed to uracil, there is a coincident conformational transition in the furanose ring from C2′ endo to C3′ endo in the methylphosphonate-substituted oligomer.

Table IV. Mean Furanose Conformations of Oligomer:Target DNA Helical Complexes as a Function of *R*-MP versus *S*-MP Substitutions in d[TpTrCrGrTr*CrCrTrC] from 200-ps Molecular Dynamics Trajectories[a]

R-MP helix			*S*-MP helix		
O1′ endo	A4–T35	C2′ endo	O1′ endo	A4–T35	C2′ endo
C3′ endo	G6–C33	C2′ endo	C3′ endo	G6–C33	C3′ endo*
C2′ endo	G8–C31	O1′ endo	C3′ endo	G8–C31	O1′ endo
C2′ endo	A10–T29	C2′ endo	C2′ endo	A10–T29	C2′ endo
C2′ endo	C12–G27	C2′ endo	C2′ endo	C12–G27	C3′ endo*
C3′ endo	G14–C25	C2′ endo	C2′ endo	G14–C25	C2′ endo
C2′ endo	A16–T23	C2′ endo	C2′ endo	A16–T23	O1′ endo

[a] C2′ endo to C3′ endo transitions are marked with an asterisk.

Discussion

These free energy simulations demonstrate that in the case of d[TTCGT*CCTC], a single *R*-MP substitution is more stable than a *S*-MP diastereomer in complementary DNA target hybridization by −3.6 kcal/mol and that thymine substitution increases the stability of the oligomer hybridization by −1.5 kcal/mol more than uracil in a *R*-MP-substituted oligomer (on a per nucleotide basis). These data are in qualitative agreement with experimental observations reported previously by Miller et al.,[1] Bower et al.,[6] and Durand et al.[2] and for stereoregular MP substitutions in oligomers and Tm measurements for a variety of similar systems reported by Lesnikowski et al.[7]

The primary mechanism underlying the greater stability of *R*-MP is due to hydrophobic hydration of the axial projecting methyl group and the lack of significant structural perturbations within the oligomer:target DNA helix. In the case of the *S*-MP diastereomer substitution in the oligomer, there is less exposure of the equatorial methyl group to the solvent since it is oriented toward the major groove of the duplex and is in closer proximity to the exposed edge of the bases in the major groove. This observation is illustrated in Figure 3, which is the time-averaged

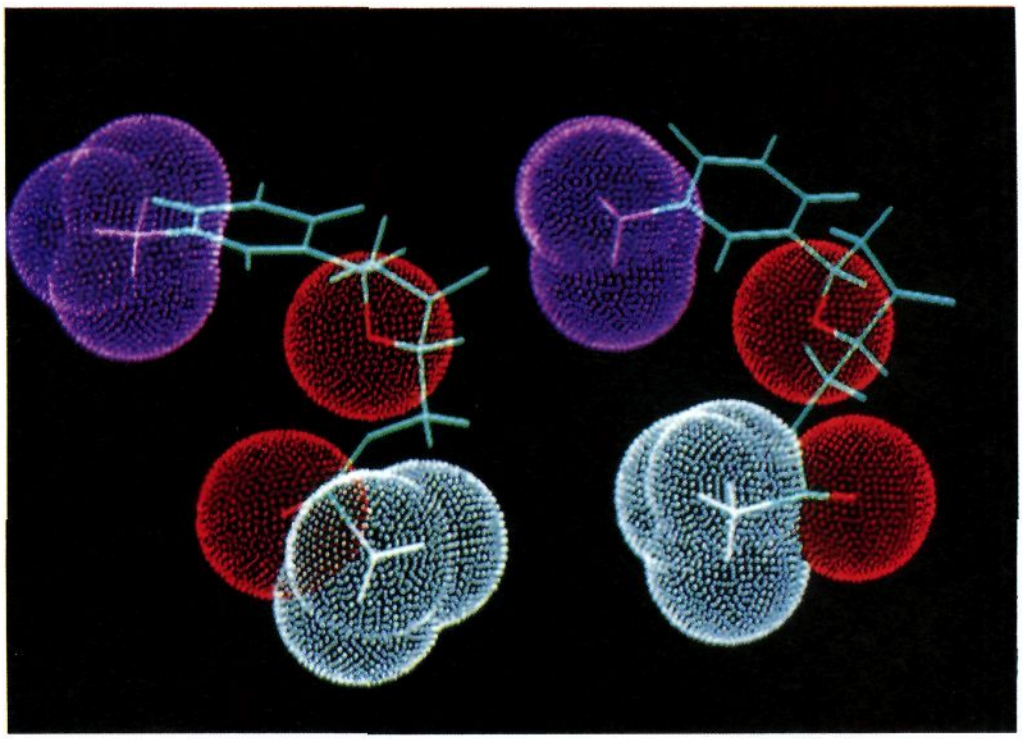

Figure 4. Comparison of the time-averaged local conformations of *R*-MP (left) and *S*-MP (right) from the DNA oligomer from the molecular dynamics trajectory. This figure illustrates the relationships between the thymine methyl groups (magenta) to the O1′ atom (red) of the furanose and the methyl groups of the MP diastereomers (white). The phosphoryl oxygen atoms are shown in red. The methyl group of the *R*-MP is rotated down and away from the O1′ atom of the furanose and the thymine methyl group. The methyl group in *S*-MP is located in proximity to the methyl group of thymine and the O1′ atom in the furanose ring. The difference in the sugar conformations in the *S*-MP and *R*-MP, as well as the accessibility of the O1′ furanose atom on the major groove side, is apparent from these time-averaged coordinates.

Table V. Mean Furanose Conformations of Oligomer:Target DNA Helical Complexes as a Function of Thymine versus Uracil Substitution in d[TpTrCrGrTr*CrCrTrC] from 200-ps Molecular Dynamics Trajectories[a]

thymine helix			uracil helix		
O1′ endo	A4–T35	C2′ endo	O1′ endo	A4–U35	C2′ endo
C3′ endo	G6–C33	C2′ endo	C3′ endo	G6–C33	C3′ endo*
C2′ endo	G8–C31	O1′ endo	C3′ endo	G8–C31	O1′ endo
C2′ endo	A10–T29	C2′ endo	C2′ endo	A10–U29	C2′ endo
C2′ endo	C12–G27	C2′ endo	C2′ endo	C12–G27	C3′ endo*
C3′ endo	G14–C25	C2′ endo	C2′ endo	G14–C25	C2′ endo
C2′ endo	A16–T23	C2′ endo	C2′ endo	A16–T23	O1′ endo

[a] Perturbed bases are underlined and local C2′ endo to C3′ endo transitions are marked with an asterisk.

conformation of the *S*-MP moiety in proximity to the furanose and thymine base. Key findings from the analysis of the time averaged coordinates of the local interactions of the *S*-MP substitution reveal that the distance between the carbon atom of the methyl group of *S*-MP and the O1′ of the furanose is only 5.46 Å (Figure 3). From Figures 3 and 4, it is apparent that the equatorial orientation of the *S*-MP methyl group hinders solvation of the O1′ furanose ring on the major groove side. As illustrated in Figure 4, the time-averaged conformation of the *S*-MP group contrasts significantly with that of the *R*-MP group. The carbon atom in the methyl group of the *R*-MP substitution faces away from the major groove side and is oriented away from the O1′ furanose atom. The distance between the O1′ atom and the carbon of the methyl group in *R*-MP is 4.82 Å, which has a closer linear proximity than the *S*-MP group configuration (Figure 4). On the basis of these data, the key difference between the localized properties of *R*-MP and *S*-MP is the difference in the major groove accessibility of O1′ which is due to the orientation of the methyl group. It is important to note in this context that methylphosphonate substitutions reduce the average number of hydrogen bonded waters from 6 (associated with the native phosphodiester oxygens) to 2.2 waters coordinated to the sp^2-hybridized phosphoryl oxygen.[10] The *S*-MP substitution produces greater disruption of the primary solvation shell, reduces the number of local waters normally surrounding the phosphodiester backbone, and specifically hinders solvation of the O1′ sugar atom on the side of the major groove.

There is a known relationship between the orientation of the methyl substituent on the phosphorus atom and DNA duplex stability, and a proposed mechanism of reduced stability of *S*-MP diastereomers is due to unfavorable local steric interactions.[6,7] Our observations suggest that the predominant mechanism leading to duplex destabilization is mediated by the following: (1) decreased solvation of the O1′ sugar atom resulting in local conformational changes in the furanose ring to C3′ endo and unwinding of the DNA helix, (2) locally destabilizing hydrophobic hydration of the methyl group of the *S*-MP backbone, and (3) weakly destabilizing intermolecular interactions between the *S*-MP methyl group and the C5 methyl group of thymine on the same strand. These events cumulatively result in localized destabilization of the DNA by *S*-MP substitution.

These simulations provide a structural basis for the alteration in hybridization stability of *R*-MP versus *S*-MP and thymine versus uracil substitutions. Target hybridization affinity is reduced by two factors: (1) helical unwinding and (2) the presence of local conformational changes in the furanose ring from B-DNA (C2′ endo) to an A-DNA (C3′ endo) within the methylphosphonate-substituted oligomer. Helical unwinding decreases the stability of the complex by producing a DNA helical hybrid which has less favorable base stacking interactions. Altering the furanose conformation from a B-DNA to an A-DNA conformation as a function of *R*-MP versus *S*-MP substitution produces a conformational hybrid within the DNA helix. In the case of the *S*-MP substitution this helical complex is composed of a B-DNA target bound by a MP oligomer with partial A-DNA behavior at the point of the *S*-MP substitution. It is notable that *N*-pucker sugars are commonly observed in B-DNA by NMR spectroscopy. In

both simulations the less energetically favored hybridized structures developed local A-DNA conformations around the perturbed site, and the on the opposite strands. Presumably the remote conformational changes identify destabilizing effects of the *S*-MP or uracil substitution in the oligomer. We cannot be certain as to the whether these additional conformational changes are a cause or a consequence of helix destabilization. Given these caveats, it is reasonable to consider that an A:B DNA hybrid is likely to be less energetically stable than a B:B DNA helix.

Hydrophobic conditions are known to promote the formation of A-DNA structures. Uracil is found in RNA, which is generally found in the A conformation, and suggests that the role of the C5 methyl group in thymine is important for maintaining a B conformation. The observation that an A-DNA furanose conformation is locally induced by the presence of the *S*-MP and with uracil substitutions facilitates further consideration of key physicochemical mechanisms which underlie the decrease in hybridization stability which accompanies these substitutions. In the case of *S*-MP, the methyl group projects equatorially in proximity over the furanose ring and decreases the solvation of the O1′ atom in the 5′ sugar.

The stability of DNA:target binding is further affected by the presence or absence of a C5 methyl group in the case of thymine or uracil, respectively. Uracil substitution in the antisense oligomer results in less stable target hybridization than thymine with an *R*-MP substitution. The mechanism underlying this decrease in complementary target stability with uracil is due to the lack of the C5 methyl group which stabilizes the hybridized oligomer to the complementary target. The C5 methyl group in thymine acts through hydrophobic hydration to drive or steady the thymine base as it binds to the DNA target. Uracil is less stable than thymine with *R*-MP substitution due to the loss of hydrophobic hydration of the C5 methyl group which reduces the stability of the oligomer:target complex. The key role of the C5 methyl group in thymine stabilizing the hybridized oligomer:target complex is further supported by the evidence from the free energy profile shown in Figure 2 that organized solvation of the C5 methyl group of thymine appears to be disrupted by the *S*-MP substitution.

The rapid peak and decay pattern of the free energy profile as the transition goes from *R*-MP to *S*-MP provides evidence that the stability of the DNA complex is modulated as a function of the orientation of the methyl group on the phosphate. There are two notable features in this profile which strongly support alterations in hydrophobic hydration modulation of DNA helical stability as a function of *R*-MP versus *S*-MP substitution: (1) the transitional slope of this free energy profile (Figure 1) is nearly a mirror image at the midpoint ($\lambda = 0.5$), comparing λ as the transition proceeds from 1 to 0.5 to that of λ as the transition proceeds from 0.5 to 0.0, and (2) the initial and final values of $\Delta\Delta G_{\text{hybrid}}$, which differ significantly with regard to the absolute value of the free energy as a function of the chemical state, which in this case is strictly only a conformational change in the orientation of the MP diastereomer which is surrounded by water.

These findings support the development of stereoselective synthesis of *R*-MP and *S*-MP incorporated into antisense oligomers and the helix that thymine will provide greater stability than uracil in the case of *R*-MP substitution adjacent to the base in the 5′ position. We are presently investigating the effects of *R*-MP versus *S*-MP in uracil-substituted antisense oligomers and studying the effects of *R*-MP versus *S*-MP as a function of nucleotide sequence at the 5′ and 3′ position relative to the methylphosphonate substitution.

The utility of free energy simulations in studying hybridization affinities of antisense oligomers to complementary genetic targets has been demonstrated for the first time. Large-scale free energy simulations to study the binding affinity of antisense oligomers to target sequences can facilitate progress in the design and optimization of critical physicochemical determinants of antisense target hybridization. With the increasing power of supercomputers, it is conceivable that larger molecular perturbations can be studied using this approach in the future and could evolve into a useful technique to guide and complement experimental studies in this and other areas.

Acknowledgment. We greatly appreciate helpful discussions with Paul Miller. All calculations were carried out on the CRAY X-MP1-16/SE at Scripps and the CRAY X-MP 14/SE and X-MP2/4 at the Center for High Performance Computing at the University of Texas System in Austin, Texas. This research was supported (F.H.H. and U.C.S.) by academic grants from Cray Research, Inc. (K-GAHM-XX-531-2-99 and K-531-1-99) and Sterling Drug, Inc. (F.H.H.).